Short Papers

Realistically Tilted and Truncated Anatomically Based Models of the Human Head for Dosimetry of Mobile Telephones

Gianluca Lazzi and Om P. Gandhi

***Abstract*—Realistically tilted models of the human head have been developed to improve the accuracy of the numerical simulation of coupling between the human head and cellular telephones for the likely tilted positions of the antennas vis à vis the head. A "best fitting" technique is used to rotate an approximately $2 \times 2 \times 3$ mm resolution model of the human head based on MRI scans of a male volunteer so that the handset may be modeled in the vertical position without stairstep approximation. With this technique, it is possible to move the head with six degrees of freedom in space, instead of the usual three, due to the simple translation therby allowing a more realistic analysis of the EM coupling between cellular telephones and the human head. Furthermore, to avoid the problem of the large amount of computer memory required for the whole head simulations, we introduced new truncated head models, and the possibility of using them was carefully analyzed. Comparisons of the SAR distributions show that it should be possible to use half head models at 835 MHz and even smaller one-third head models at the Personal Communications Services (PCS) frequency of 1900 MHz. It is shown that, by using the truncated one-third model, it is possible to run with just 42 Mbytes of memory a case that originally needed 85 Mbytes. The truncated models should help to render these large SAR analyses doable by most of the commonly available workstations.**

I. Introduction

For the last few years, there has been public concern about the possible health risks associated with the use of handheld mobile telephones. Because of this, considerable effort has gone into improving the capabilities of computer simulations and experimental techniques for quantifying the electromagnetic absorption from such devices. Unfortunately, both experimental and numerical simulations have some limits. For experimental setups, a major issue is to prove the adequacy of the available simplified phantoms to model the real head. Numerical simulations, on the other hand, are often criticized because they do not guarantee a proper model of the internal substructures of the cellular telephone and a correct tilted position of the telephone vis à vis the head. Even though several positions and models of the telephones have been used in the past [1], and a tilted head model has been used in [2], a realistic head tilting has never been carefully described. Our past attempts at tilting the model by displacing each successive layer of the magnetic resonance imaging (MRI) scans back by one cell [3] have led to unsatisfactory distortion of the head. To model realistic positions of the telephone relative to the head, we have decided to tilt the MRI-based model of the head and neck forward by 30° with or without an additional rotation of 9° in the plane normal to the face. This allows modeling of the handset and the antenna as though they were held in the vertical position, which eliminates having to resort to the use of stairstepped cells. Stairstepped cells constitute a source of error [4]–[6] which is thus avoided in modeling linear types of mobile telephone antennas. Moreover, keeping the telephone vertical will render easier the modeling of new antennas, such as microstrip antennas. Both of the forward tilted models allow us to calculate the specific absorption rate (SAR) distributions using positions that are representative of a person holding a cellular telephone. A further rotation of 9° in the right angle plane allows modeling the mouthpiece of the telephone close to the lower jaw. The peak 1-g average SARs as well as the average SARs in the most important organs are investigated to understand the influence of the position of the head in the calculation of these parameters.

TABLE I
Dielectric Properties [10] and Specific Gravities of the Various Tissues Assumed at the Midband Mobile Telephone Frequencies of 835 and 1900 MHz

Tissue	Spec. Gravity 10^3kg/m^3	835 MHz ε_r	835 MHz σ S/m	1900 MHz ε_r	1900 MHz σ S/m
muscle	1.04	51.76	1.11	49.41	1.64
fat	0.92	9.99	0.17	9.38	0.26
bone (skull)	1.81	17.40	0.25	16.40	0.45
cartilage	1.10	40.69	0.82	38.10	1.28
skin	1.01	35.40	0.63	37.21	1.25
nerve	1.04	33.40	0.60	32.05	0.90
blood	1.06	55.50	1.86	54.20	2.27
parotid gland	1.05	45.25	0.92	43.22	1.29
CSF	1.01	78.10	1.97	77.30	2.55
eye humour	1.01	67.90	1.68	67.15	2.14
sclera	1.17	54.90	1.17	52.56	1.73
lens	1.10	36.59	0.51	42.02	1.15
pineal gland	1.05	45.26	0.92	43.22	1.29
pituitary gland	1.07	45.26	0.92	43.22	1.29
brain	1.04	45.26	0.92	43.22	1.29

To calculate the SAR distributions for all of the above cases, we have used the finite-difference time-domain (FDTD) method that is widely used for solving many types of electromagnetic problems [7], [8]. The accuracy of the FDTD code has previously been investigated [3], [7]–[9] and will not be reported here. For the present calculations, we have used a millimeter-resolution model of the human head based on the MRI scans of a male adult volunteer [3], [9]. A voxel (volume pixel) size of $1.974 \times 1.974 \times 3$ mm and 15 different tissue types were used in the simulations. The dielectric properties available from the most recent data [10] were assigned to each of the tissues and are given in Table I.

It is recognized that the present model with a resolution of 3 mm in the vertical direction does not satisfy the requirement that the cell size be less than $\lambda_\varepsilon/10$ in each direction. It has, however, been shown previously [11] that cell sizes as large as $\lambda_\varepsilon/5$ are capable of giving fairly accurate SAR distributions. We therefore consider the present model with a resolution of 2–3 mm to be adequate to about 2000 MHz. For higher-frequency applications it would be necessary to use finer-resolution models, and one such model with a cubical cell size of 0.9375 mm is presently under development

Manuscript received January 31, 1996; revised October 9, 1996.

The authors are with the Department of Electrical Engineering, University of Utah, Salt Lake City, UT 84112 USA.

Publisher Item Identifier S 0018-9375(97)01781-X.

in our laboratory. To save computer memory for the present model as well as allow use of the higher resolution models in the future, we have investigated the use of truncated head models. Observing that the distal side of the head is usually relatively shielded from the EM fields generated by the telephone, another source devoid of RF power may be symmetrically placed on the opposite side without a significant alteration of the results. This new problem can be studied by superposing the results obtained with an "even" simulation and an "odd" simulation performed, respectively, using a perfect magnetic conductor (PMC) and a perfect electric conductor (PEC) at the plane of symmetry of the head [12]. With this technique, we have considered also the possibility of using a one-third head model which has been found to be accurate at the PCS frequency of 1900 MHz. To quantify the errors obtained with the truncated models relative to the full head model, we have defined a correlation coefficient that can assume values between -1 (complete disagreement of data) and 1 (complete agreement of data). Correlation coefficients of the order of 0.996 to 0.999 have been obtained for all of the acceptable truncated models. Computer memories of the order of 60 and 50% are needed for one-half and one-third models of the head, respectively. Because of the need to also model the cellular telephone, the hand and the region to the absorbing boundaries, savings in memory commensurate to the reduced models of the head are obviously not obtained. These simulations, possible to date only by the use of workstations with considerably large random access memory (RAM), may then be run on most of the commonly available workstations.

II. Tilted Head Models

To obtain the tilted head models, the original model based on the MRI scans of an adult male was rotated cell by cell. Due to the discretization, a partial overlap in mapping between two or more cells may be experienced in this process. To avoid this problem, a matrix of what we called "mapping errors" was built: Every cell was assigned to a new corresponding cell only if no other cells had a better fitting to the new one. In particular, we considered a cell mapping to have 0% error when the center of the original cell is mapped to the center of the new cell, and 100% error when the center of the cell is mapped to one of the corners of the new cell. An intermediate error proportional to the distance of the mapped position of the cell centroid from the center of the new cell is then assigned with the higher value of, say, 99.9% assigned for each of the neighbors to form the matrix of the mapping errors. When each of the original cells is rotated, the element of the matrix of the mapping errors corresponding to the new calculated element is checked. If the obtained error is less than those stored in the mapping errors matrix, this cell substitutes the previous one in the destination location. The high percentage error assigned to the neighbors guarantees an occupancy of this cell by the mapped tissue only in the case that no other cells that fit this new one are found. The models were checked in their layers and compared with the original model. Some minor modifications were also performed manually.

With this technique, the model of 30° forward-tilted head and 30° forward-tilted head with a further 9° rotation of the face toward the mouthpiece of the telephone was obtained. Fig. 1 shows the three models with the telephone. As seen in Fig. 1(a), where the x-, y-, and z-axes are marked, the 30° tilting corresponds to a rotation of 30° in the y-z plane [Fig. 1(b)]. The 30° forward-tilted head with further rotation of 9° of the face is created by a two-step process: First, the head is tilted 30° in the y-z plane, and then rotated 9° in the x-z plane. Table II shows the number of cells for each of the 15 tissues for the three models (vertical, tilted 30°, and tilted 30° with 9° rotation toward the telephone). As can be seen, the differences in tissue content between the tilted head models and the original vertical model are not significant, and this is a direct consequence of the discretization scheme suggested here.

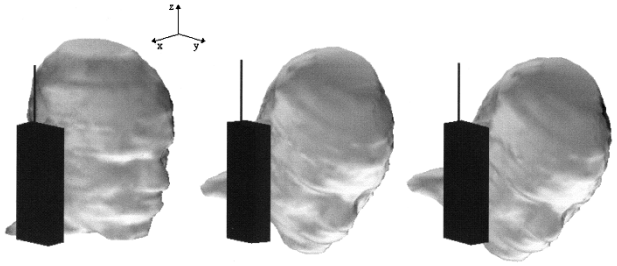

Fig. 1. Visualization of the various segmented head models with the telephone: Vertical, tilted 30°, and tilted 30° with a further rotation of 9° of the face toward the telephone.

TABLE II
Number of Cells for Each of the Tissues for All the Considered Models of the Head: Vertical, Tilted 30°, and Tilted 30° with a Further Rotation of 9° of the Face

Tissue	Vertical Head Model	Tilted 30° Head Model	Tilted 30° Head Model, with Further Rotation of 9°
muscle	104,690	107,731	107,700
fat	70,866	72,272	72,209
bone	82,298	82,673	82,647
cartilage	3,595	3,665	3,646
skin	29,626	30,261	30,263
nerve	1,719	1,756	1,747
blood	3,676	3,697	3,660
parotid gland	149	143	142
CSF	1,742	1,713	1,717
eye humour	1,464	1,488	1,486
sclera	848	843	852
lens	160	164	163
pineal gland	18	16	16
pituitary gland	22	24	24
brain	138,188	138,124	138,198

In all of the considered models, the ear near the telephone has been compressed by the pressure of the telephone. This means that the top part of the left ear was shifted inward to touch the scalp. The modification involved a few cells, and the result was monitored carefully to be sure that the ear assumed a position simulating a person holding a cellular telephone. In the model of the tilted head with the lower jaw closer to the telephone, the ear was slightly modified with respect to the other two cases to take into account the fact that, in this case, the top of the ear is less compressed while the bottom is more compressed. The difference was limited to few cells and the modification was necessary to ensure the full contact of the telephone with most of the surface of the ear, as for the other two cases.

III. Truncated Head Models

The amount of computer memory necessary for these simulations is fairly large, usually of the order of 100 Mbytes. Because of the larger parallelepipeds that must be used, the tilted head models, in particular, require much larger volumes to be discretized than for simple vertical models. Such large models challenge even extremely

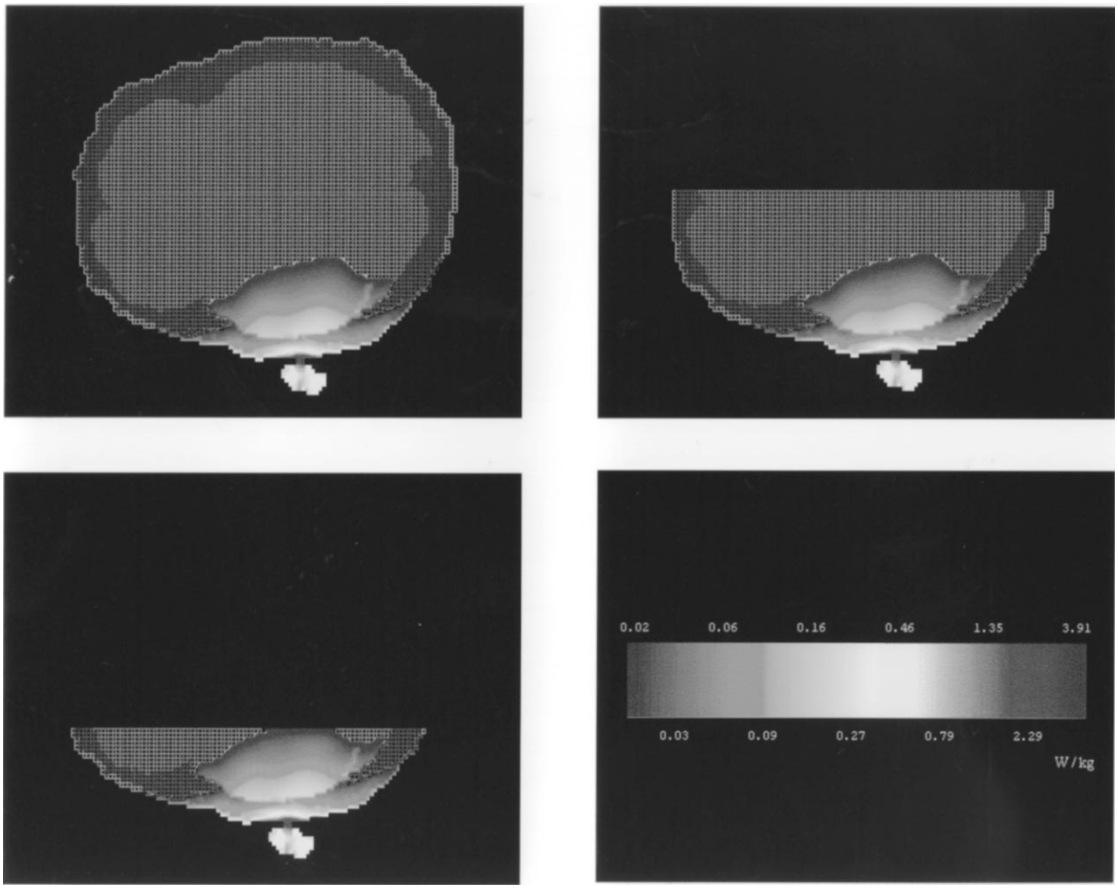

Fig. 2. SAR distribution in layer #34 (10.05 cm below the top of the head) for the vertical head model for the three considered cases: full model, truncated half model, and truncated one-third model. Radiated frequency = 1900 MHz, $\lambda/4$ antenna, input power = 125 mW.

sophisticated workstations at the present time. Considering that the desire is to move in the future toward models with resolution of the order of $1 \times 1 \times 1$ mm, a way to save computer resources becomes particularly important. In this section, we investigate the possibility of using truncated models of the head to save considerable computer memory without a significant loss in accuracy.

As mentioned in Section I, the basic idea and assumption is that a dummy telephone devoid of RF power, placed symmetrically on the distal side of the head, does not affect the field distribution, especially for the region proximal to the powered mobile telephone where the highest SARs are found.

Considering that the head is symmetric with respect to the telephones, this modified situation can be conveniently analyzed by superimposing the results of two simpler simulations, "even" and "odd." The first case corresponds, physically, to the situation in which the telephones are provided with RF power in phase, and can be analyzed by placing a PMC at the plane of symmetry of the head. Similarly, the "odd" case corresponds to the situation in which the telephones are provided with RF power out of phase, and can be analyzed by placing a PEC at the plane of symmetry of the head. The procedure was also extended to one-third head models. In both half- and one-third model cases, the superposition is obtained by summing the even and odd cases with the same weight.

We can compare the two SAR distributions f and p corresponding to the full model and the truncated partial model by means of an ensemble correlation coefficient. If f_i and p_i represent, respectively, the SAR values obtained for the full model and the truncated partial model at the same cell location i, an ensemble correlation coefficient may be defined as follows [13]

$$r = \frac{\sum_{i=1}^{n}(f_i - \bar{f})(p_i - \bar{p})}{\sqrt{\sum_{i=1}^{n}(f_i - \bar{f})^2}\sqrt{\sum_{i=1}^{n}(p_i - \bar{p})^2}}$$

where $\bar{f}$ and $\bar{p}$ are, respectively, the average of the values f_i and p_i. It is important to observe that

1) r is independent from the labeling of f and p;
2) r is independent of the units in which f and p are measured;
3) r is between -1 and 1;
4) $r = 1$ if all (f_i, p_i) pairs lie on a straight line with positive slope, and $r = -1$ if all (f_i, p_i) pairs lie on a straight line with negative slope.

The ensemble correlation coefficient was introduced to provide an estimate of the difference in SARs between truncated and full models. This is because not only is the 1-g average SAR important, but also the local SARs and SARs in particular organs are often of interest. The correlation coefficient shows the reliability of the truncated models to predict the correct SAR distribution for the complete model.

Additional useful information can be obtained by considering the set of data obtained by the difference of the SAR, calculated cell by cell, between the distribution associated with the full model and that associated with the truncated partial model, i.e., $(f_i - p_i)$. For perfect coincidence of the two distributions, both the average and the variance of these quantities for the entire ensemble should be zero.

Other techniques were tried in the past by our group, but results were never satisfactory. In particular, the most simple truncation realized by simply cutting off part of the model and using air

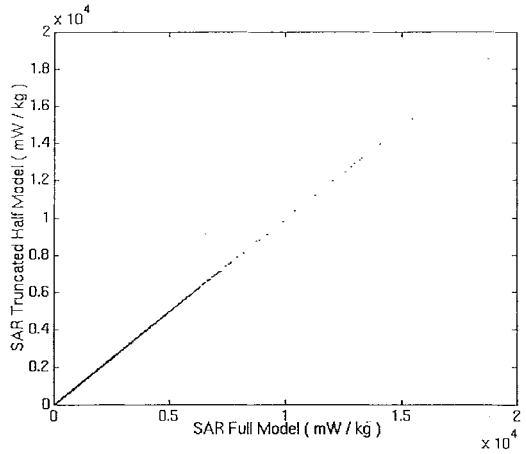

(a)

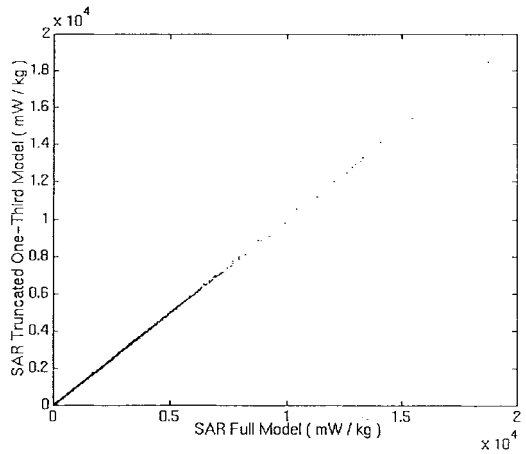

(b)

Fig. 3. Scatter plot of the individual cell SARs obtained for the full model for 1900 MHz, $\lambda/4$ antenna, versus the corresponding values obtained with the use of the truncated half model [Fig. 3(a)] and the truncated one-third model [Fig. 3(b)]. Radiated power = 125 mW.

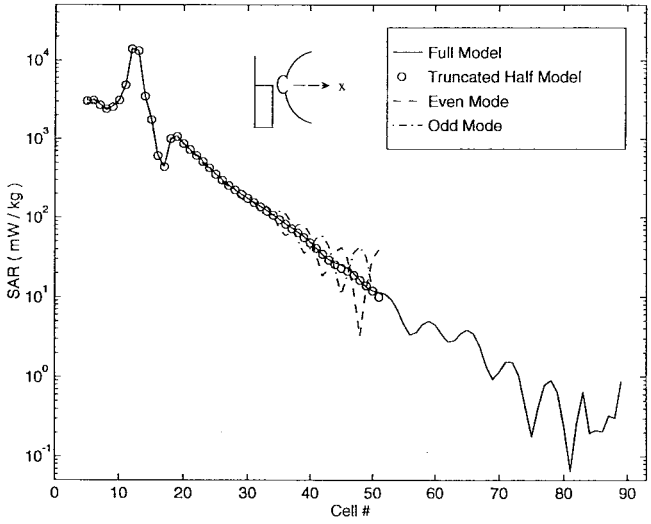

(a)

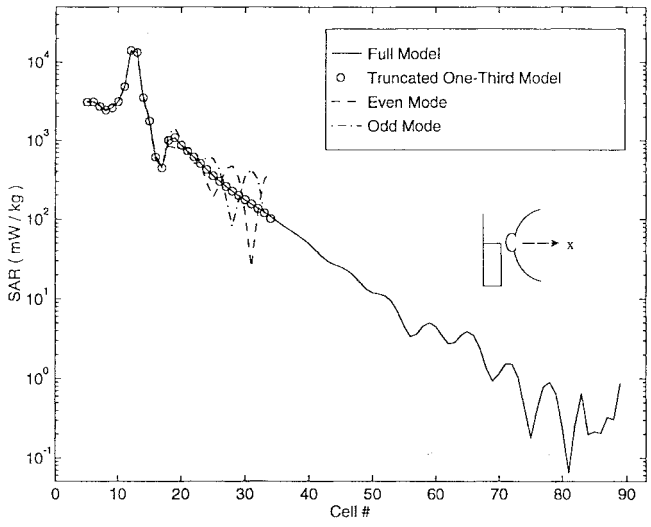

(b)

Fig. 4. SARs along the x-direction in line with the source point for the full model, the truncated model, the even-only simulation, and the odd-only simulation obtained with the use of the half model [Fig. 4(a)] and the use of the one-third model [Fig. 4(b)]. Frequency = 1900 MHz, $\lambda/4$ antenna, radiated power = 125 mW.

before the absorbing boundaries produced reflections at the tissue-air interface. Also, fields from the source were able to creep around the models and produced SARs on the back side. Furthermore, as seen in Fig. 4(a) and (b), the use of only even simulation (defined in the past as "continuation of the fields" technique) produces results that are considerably less accurate than those provided by the superposition of the even and odd simulations, especially near the truncation boundaries [12].

IV. Results

To evaluate the influence of the position of the head relative to the telephone an important parameter to consider is the peak 1-g SAR. The ANSI-IEEE C95.1-1992 standard [14] prescribes a value of 1.6 W/kg for any 1-g of tissue as a limit value for uncontrolled environments.

Table III shows the comparison for the peak 1-g SAR and the peak 1-g brain SAR, calculated at 835 and 1900 MHz, for the three full-head models described above. A metal box telephone of dimensions 2.76 × 5.53 × 15.3 cm (14 δ_x × 28 δ_y × 51 δ_z with a 1 mm thick plastic covering of relative dielectric constant $\varepsilon_r = 4.0$ is considered for each of the cases. The antenna is a $\lambda/4$ monopole mounted on the back side, center position of the telephone (away from the head). The radiated power for the data shown in Tables III–VII is assumed to be 600 mW at 835 MHz and 125 mW at 1900 MHz. The total radiated power can be calculated in two ways. The first method calculates the total power as the sum of the radiated power and the power absorbed by the head and the hand. This gives the total power radiated by the telephone, and the SAR values at the required powers can be obtained by simply scaling the calculated values by the ratio of the required power (600 or 125 mW) and the calculated power. The second method is to calculate the radiated power at the antenna feed point and scale the SAR values as explained above. We calculated the radiated power for the full models both ways to verify the accuracy of the code, and we always obtained a difference between the two methods of less than 1% for the antennas considered in this paper. For the case of the truncated models, however, the power was calculated by only the second method because of the difficulties in calculating the overall power absorbed by the head using the first method. As further confirmation of the accuracy of the second method, the radiated powers calculated using the truncated models were always extremely close to the ones obtained using full-model runs.

TABLE III
PEAK 1-g SAR'S FOR THE HEAD AND THE BRAIN IN W/kg AT 835 AND 1900 MHz FOR THE THREE CONSIDERED HEAD MODELS. GIVEN IN PARENTHESES ARE THE ACTUAL WEIGHTS OF THE SUBVOLUMES CONSIDERED FOR THE PEAK 1-g SAR's. THE TELEPHONE IS ASSUMED TO BE A PLASTIC-COVERED METAL BOX WITH A $\lambda/4$ MONOPOLE ANTENNA MOUNTED ABOVE IT. THE RADIATED POWER IS ASSUMED TO BE 600 mW AT 835 MHz AND 125 mW AT 1900 MHz

Frequency (MHz)		Vertical Head Model	Tilted 30° Head Model	Tilted 30° Head Model, with Further Rotation of 9°
835	Peak 1-g SAR for head	2.93 (1.01 g)	2.44 (1.03 g)	2.31 (1.10 g)
	Peak 1-g SAR for brain	1.13 (1.09 g)	0.93 (1.02 g)	0.66 (1.00 g)
1900	Peak 1-g SAR for head	1.11 (1.03 g)	1.08 (1.03 g)	1.20 (1.01 g)
	Peak 1-g SAR for brain	0.19 (1.00 g)	0.20 (1.04 g)	0.16 (1.02 g)

TABLE IV
AVERAGE SAR'S IN SELECTED TISSUES AT 835 AND 1900 MHz FOR THE THREE CONSIDERED HEAD MODELS. THE TELEPHONE IS THE SAME AS FOR TABLE III

Frequency (MHz)	Average SARs (mW/kg)	Vertical Head Model	Tilted 30° Head Model	Tilted 30° Head Model, with Further Rotation of 9°
835	Brain	72.3	60.6	49.1
	CSF	72.7	66.4	53.7
	Eye humour	31.8	20.6	20.7
1900	Brain	7.6	7.0	7.2
	CSF	7.9	6.7	7.9
	Eye humour	3.2	1.2	1.7

In Table III it is interesting to note that at 835 MHz the peak 1-g SAR and the peak 1-g SAR for the brain are both highest for the case of the vertical head and lowest for the case of the tilted 30° head with the further rotation of 9° toward the telephone. The 30° tilted head model gives results intermediate to the other two cases. It is not surprising that the vertical head model gives the highest 1-g SAR for head and brain because this is the situation with the closest coupling between the head and the antenna. In the other two cases, the results are lower because the antenna is somewhat further from the head. In particular, the model with the lower jaw close to the telephone has the scalp with a larger distance from the antenna. Similar considerations are not valid at 1900 MHz, likely due to the very short dimensions of the antenna. In this case, the coupling between the head and the antenna remains almost the same for all the considered models. A similar trend can also be observed for the average SARs in some of the selected tissues, as shown in Table IV.

Several test runs were also performed to verify the accuracy of using the truncated head models. Table V shows the peak 1-g SAR's for the head and the brain obtained at 835 and 1900 MHz with the use of the vertical head model. Antennas of length $\lambda/4$ and $3\lambda/8$ are considered for these calculations. All three models, full, truncated half, and truncated one-third, are compared. The correlation coefficient with the full model is also reported for each of cases as a measure of the accuracy of the truncated models vis à vis the full model. As expected, better results are obtained at 1900 MHz due to the relatively shallow penetration of the energy in the head at this frequency. Also, because of the shorter dimensions of the antenna, the coupling between the physical antenna and the "virtual" symmetric

TABLE V
PEAK 1-g SAR'S FOR THE HEAD AND THE BRAIN IN W/kg OBTAINED AT FREQUENCIES OF 835 AND 1900 MHz FOR THE VERTICAL TRUNCATED HEAD MODELS. THE TELEPHONE IS A PLASTIC-COVERED METAL BOX WITH $\lambda/4$ OR $3\lambda/8$ MONOPOLE ANTENNA MOUNTED ABOVE IT. THE RADIATED POWER IS ASSUMED TO BE 600 mW AT 835 MHz AND 125 mW AT 1900 MHz

Frequency (MHz)	Antenna		Vertical Head Model	Vertical Half Head Model	Vertical One-Third Head Model
835	λ/4	Peak 1-g SAR for head	2.93 (1.01 g)	2.86 (1.01 g)	2.84 (1.01 g)
		Peak 1-g SAR for brain	1.13 (1.09 g)	1.09 (1.09 g)	1.23 (1.09 g)
		Corr. Coeff.	–	0.99948	0.99614
	3 λ/8	Peak 1-g SAR for head	1.60 (1.01 g)	1.62 (1.01 g)	1.80 (1.01 g)
		Peak 1-g SAR for brain	0.65 (1.05 g)	0.69 (1.00 g)	0.93 (1.05 g)
		Corr. Coeff.	–	0.99655	0.98911
1900	λ/4	Peak 1-g SAR for head	1.11 (1.03 g)	1.10 (1.03 g)	1.10 (1.03 g)
		Peak 1-g SAR for brain	0.19 (1.00 g)	0.19 (1.00 g)	0.19 (1.00 g)
		Corr. Coeff.	–	0.99999	0.99991
	3 λ/8	Peak 1-g SAR for head	0.69 (1.06 g)	0.68 (1.06 g)	0.69 (1.06 g)
		Peak 1-g SAR for brain	0.16 (1.00 g)	0.16 (1.00 g)	0.16 (1.00 g)
		Corr. Coeff.	–	0.99961	0.99943

antenna is very low. At 835 MHz the results remain fairly good with the exception of the case with the $3\lambda/8$ antenna and the one-third model. In this case, the long antenna is not well shielded by the head and the dummy telephone is relatively near to the real source.

Fig. 2 shows the SAR deposition in layer #34 for the full model, the truncated half model, and the truncated one-third model with a $\lambda/4$ antenna, a radiated input power of 125 mW, and a frequency of 1900 MHz. As can be seen, the SAR distribution for all the three cases is nearly identical. It is interesting to note that even though the SAR values at the truncated boundary for the one-third model are on the order of 0.5–1% of the peak SAR, no reflections arise and no hot spots are present.

Table VI shows the calculated results for the truncated models of the tilted head. Once again, the assumed antenna is a $\lambda/4$ monopole, at 835 and 1900 MHz. In this case the one-third model does not provide very satisfactory results at 835 MHz, while at 1900 MHz both one-half and one-third models give results close to those obtained for the full models.

Fig. 3 shows the scatter plot of the individual cell SARs obtained for the full model at 1900 MHz, $\lambda/4$ antenna, versus the corresponding values obtained with the use of the truncated half model [Fig. 3(a)] and the truncated one-third model [Fig. 3(b)]. For exact correspondence of SARs—cell by cell—of the full model and the truncated models, all the points should lie on the straight line with a slope of 45°. As can be seen, in both cases no points depart from this line, and this confirms the result obtained with the use of the correlation coefficient.

Fig. 4 depicts the SAR along a line corresponding to the source point for the full model, the truncated model, the even simulation, and the odd simulation obtained with the use of the truncated half model [Fig. 4(a)] and the use of the truncated one-third vertical head model [Fig. 4(b)] at 1900 MHz. A 6-cycle log scale is used in order to compare the SARs over a wide range, including the values at deeper locations that are fairly small in comparison with the surface SARs. The even and odd simulations done individually show oscillations

TABLE VI
PEAK 1-g SAR'S FOR THE HEAD AND THE BRAIN IN W/kg OBTAINED AT FREQUENCIES OF 835 AND 1900 MHz WITH THE USE OF THE TILTED TRUNCATED HEAD MODELS. THE TELEPHONE IS THE SAME AS FOR TABLE III

Frequency (MHz)	Model	Peak 1-g SAR Head(W/kg)	Peak 1-g SAR Brain (W/kg)	Correlation Coefficient
835	A	2.44 (1.03 g)	0.93 (1.02 g)	–
	A, Half Head Model	2.44 (1.03 g)	0.91 (1.02 g)	0.99969
	A, One-Third Head Model	2.60 (1.03 g)	1.06 (1.02 g)	0.99356
	B	2.31 (1.10 g)	0.66 (1.00 g)	–
	B, Half Head Model,	2.30 (1.10 g)	0.64 (1.00 g)	0.99951
	B, One-Third Head Model	2.67 (1.10 g)	0.88 (1.00 g)	0.99179
1900	A	1.08 (1.03 g)	0.20 (1.04 g)	–
	A, Half Head Model	1.08 (1.02 g)	0.20 (1.04 g)	0.99990
	A, One-Third Head Model	1.08 (1.02 g)	0.20 (1.04 g)	0.99976
	B	1.20 (1.01 g)	0.16 (1.02 g)	–
	B, Half Head Model,	1.17 (1.01 g)	0.16 (1.00 g)	0.99760
	B, One-Third Head Model	1.16 (1.01 g)	0.15 (1.00 g)	0.99719

Model A: Tilted 30° Head Model
Model B: Tilted 30° Head Model with further rotation of 9°

near the tail of the curves, while the superposition is able to follow accurately the full model distribution for all of the curve. Similar trends were obtained for all the considered cases.

Finally, Table VII shows the summary of the required computer memory for all the considered cases. The global saving obtained with the one-third models in respect to the memory necessary for the full simulation is up to 52%. The reported memory usage has been obtained practically leaving in the computer memory only the field arrays necessary for the FDTD algorithm, and the array in which the dielectric properties of each cell are stored. The SARs have been obtained with a post-processor after saving the necessary field components obtained by the FDTD code on the disks. In particular, the calculation of the amplitude and phase of each field component for all the FDTD cells requires the solution of two equations in two unknowns from the knowledge of values at two different time instants, since every field component is sinusoidal in steady state [15]. Therefore, two values obtained typically 25 time steps apart for each field component in each cell are stored on disk. The post-processor, when the truncated models are used, should first calculate the amplitudes and relative phases of the peak fields for the even and the odd simulations, add the two, and then calculate the SARs.

V. CONCLUSION

Realistically tilted models of the human head presented and used for simulations of the EM absorption from mobile telephones are significantly more accurate than those used to date. The position of the head relative to the telephone can now be considered to be very close to the true position used by a person holding the telephone. Results show that, at 835 MHz, lower peak 1-g SAR's were obtained

TABLE VII
THE REQUIRED COMPUTER MEMORY IN MBYTES FOR THE FULL AND THE TRUNCATED HEAD MODELS. GIVEN IN PARENTHESES ARE THE MESH SIZES FOR EACH OF THE CONSIDERED CASES

	Full Model	Half Model	One-Third Model
Head Model	84 ($153 \times 154 \times 117$)	51 ($91 \times 154 \times 117$)	42 ($74 \times 154 \times 117$)
Tilted 30° Head Model	111 ($153 \times 173 \times 140$)	68 ($91 \times 173 \times 140$)	56 ($74 \times 173 \times 140$)
Tilted 30° Head Model, with Further Rotation of 9°	116 ($160 \times 173 \times 140$)	68 ($91 \times 173 \times 140$)	56 ($74 \times 173 \times 140$)

for tilted head models vis à vis the simple vertical position, while the same effect was not observed at 1900 MHz due to the very short length of the antenna. The possibility of using truncated head models was carefully analyzed. It is shown that the truncated half model produces results within a few percent for all of the considered cases. At 1900 MHz, the one-third model also provides accurate results. This will allow a considerable saving in computer resources without significant loss in accuracy.

ACKNOWLEDGMENT

The authors would like to thank C. M. Furse for invaluable suggestions and helpful comments and anonymous reviewer no. 2. Both contributed to considerably improve the presentation of the manuscript.

REFERENCES

[1] P. J. Dimbylow and S. M. Mann, "SAR calculations in an anatomically based realistic model of the head for mobile communication transceivers at 900 MHz and 1.8 GHz," *Phys. Med. Biol.*, vol. 39, pp. 1537–1553, 1994.
[2] M. A. Jensen and Y. Rahmat-Samii, "EM interaction of handset antennas and a human in personal communication," *Proc. IEEE*, vol. 83, pp. 7–17, 1995.
[3] O. P. Gandhi, and J. Y. Chen, "Electromagnetic absorption in the human head from experimental 6 GHz handheld transreceiver," *IEEE Trans. Electromag. Compat.*, vol. 37, pp. 547–558, Nov. 1995.
[4] R. Holland, "Pitfalls of staircase meshing," *IEEE Trans. Electromag. Compat.*, vol. 35, pp. 434–439, 1993.
[5] R. Holland, V. P. Cable, and L. C. Wilson, "Finite-volume time-domain (FVTD) techniques for EM scattering," *IEEE Trans. Electromag. Compat.*, vol. 33, pp. 281–294, 1991.
[6] A. C. Cangellaris and D. B. Wright, "Analysis of the numerical error caused by the stair-stepped approximation of a conducting boundary in FDTD simulations of electromagnetic phenomena," *IEEE Trans. Antennas Propagat.*, vol. 39, pp. 1518–1525, 1991.
[7] K. S. Kunz and R. J. Luebbers, *The Finite-Difference Time-Domain Method in Electromagnetics*. Boca Raton, FL: CRC, 1993.
[8] A. Taflove, *Computational Electrodynamics: The Finite-Difference Time-Domain Method*. Dedham, MA: Artech House, 1995.
[9] O. P. Gandhi, "Some numerical methods for dosimetry: extremely low frequencies to microwave frequencies," *Radio Sci.*, vol. 30, pp. 101–177, 1995.
[10] C. Gabriel, "Compilation of the dielectric properties of body tissues at RF and microwave frequencies," *Final Tech. Rep. AL/OE-TR-1996-0037*, Occupational and Environmental Health Directorate, RFR Division, Brooks AFB, TX 78235-5102, June 1996.
[11] O. P. Gandhi, Y. G. Gu, J. Y. Chen, and H. I. Bassen, "Specific absorption rates and induced current distributions in an anatomically based human model for plane-wave exposure," *Health Phys.*, vol. 63, pp. 281–290, 1992.
[12] O. P. Gandhi, G. Lazzi, and C. M. Furse, "Electromagnetic absorption in the human head and neck for mobile telephones at 835 and 1900 MHz," *IEEE Trans. Microwave Theory Tech.*, vol. 44, pp. 1884–1897, Oct. 1996.

[13] J. L. Devore, *Probability and Statistics for Engineering and the Sciences*, 2nd ed. Belmont, CA: Brooks/Cole, 1987.
[14] *American National Standards Institute—Safety Levels With Respect to Exposure to Radio Frequency Electromagnetic Fields, 3 kHz to 300 GHz*, ANSI/IEEE C95.1-1992.
[15] C. M. Furse, J. Y. Chen, and O. P. Gandhi, "Calculation of electric fields and currents induced in a millimeter-resolution human model at 60 Hz using the FDTD method with a novel time-to-frequency-domain conversion," submitted for publication.

Isotropic Receive Pattern of an Optical Electromagnetic Field Probe Based Upon Mach-Zehnder Interferometer

Serigne Diba and Hubert Trzaska

***Abstract*—This article describes a new idea for the design of electric field sensors that is informative for engineers studying sensors. However, there was no experiment to show that such a sensor can be made. The phase difference between light waves at the output ports of the sensors should be considered to realize the sensor. This article is devoted to an optical electromagnetic field probe based on Mach-Zehnder interferometer. Unlike the electric sensors based on diode dipole technology, obtaining an isotropic receive pattern, in the case of an optical electromagnetic field probe, requires the use of three appropriately biased sensors connected in parallel before scaler summation. The configuration of such a sensor is being discussed in this article.**

I. Introduction

The recent achievements made in the field of EMC and the necessity to protect biological subjects and natural environment against harmful effects of the electromagnetic field (EMF) require the utilization of more sensitive small size EMF sensors for the measurements of emission, susceptibility, and shielding performance of different electronic and electric devices, and for the determination of electric and magnetic field intensity in a small region [6]. Similar requirements are also needed for labor safety and general public protection against undesirable exposure to EMF or the measurement of electromagnetic pulses.

Therefore, the necessity of building sensors for the measurement of EMF characterized by great accuracy and high sensitivity has become a fundamental problem, especially in the near field in which the majority of the EMF measurements for these purposes are carried out.

In near field measurements, obtaining an electric electromagnetic field probe with an isotropic receive pattern requires to raise to the power of two three spatial components of EMF before summation [5]. The configuration of an isotropic electric field meter using bulk crystal $LiNbO_3$ used in near field investigations has been fabricated at the NIST [12]. Here, the authors propose an original, attractive, and quite simple method of obtaining an electromagnetic field probe with an isotropic receive pattern. It consists of a parallel connection of three appropriately biased optical sensors before scaler summation.

Manuscript received April 20, 1996; revised November 15, 1996.
The authors are with the Institute of Telecommunications and Acoustics, Technical University of Wroclaw, 50-370 Wroclaw, Poland.
Publisher Item Identifier S 0018-9375(97)01785-7.

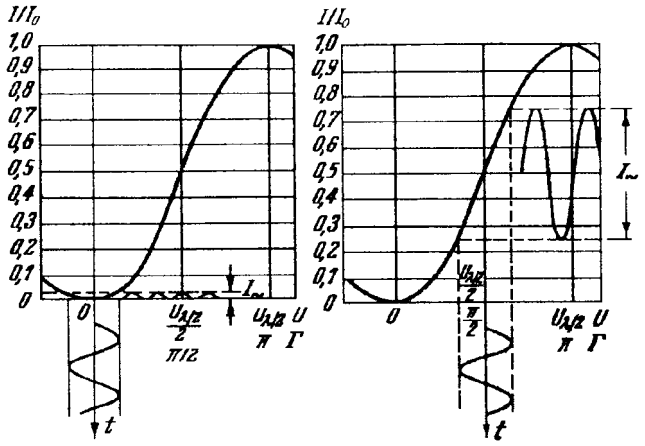

Fig. 1. Transmission factor (I_o/I_i) against voltage U.

II. Configuration of Sensor With an Isotropic Receive Pattern

In the near field, the EMF is determined by the measurement of its three components (E_x, E_y, E_z). In order to measure the three components of the investigated EMF, sensors with an isotropic receive pattern should be used. In the case of diode dipole sensors, the connection of three orthogonal dipoles with a direct current summation can provide a spherical receive pattern [5]. Obtaining an isotropic receive pattern, in the case of optical sensors, requires to use three appropriately biased sensors connected in parallel and after a scaler summation of intensities. The role of biased modulators used in the system is to deliver a squared signal at their output before summation. The properties of a biased modulator can be observed in the graph of the transmission factor of the electro-optic modulator presented in Fig. 1 [1].

It can be seen from the graph that the signal at the output of an appropriately biased modulator (for example for $V = 0$) is square law and this property is used in the configuration of the optical electromagnetic field probe's receive patterns. The configuration providing an isotropic receive pattern is discussed below.

The output signal can be expressed in terms of the input signal by the following relationship [11]:

$$P_o = \frac{1}{2} P_i [1 + \cos(\Gamma + \phi)] \tag{1}$$

where

Γ—is the component of phase difference due the applied voltage across the modulator;
ϕ—is the component of phase difference due to the bias point of the modulator with zero applied voltage $(V = 0)$.

When the modulator is biased at the operating point $\phi = \pi$, which means that the modulator has a very low sensitivity and will function adequately only in quite large fields, then the output power is equal to

$$P_o = \frac{1}{2} P_i (1 - \cos \Gamma). \tag{2}$$

The Maclaurin series representation for $\cos x$ is given by the following formula [10]

$$\cos x = 1 - \frac{x^2}{2!} + \frac{x^4}{4!} - \frac{x^6}{6!} + \cdots + (-1)^n \frac{x^{2n}}{(2n)!} + \cdots \tag{3}$$

for the interval of convergence $(-\infty, \infty)$.